768

SIMULATING WIND POWER DENSITY AROUND BUILDINGS FOR SITING BUILDING INTEGRATED WIND TURBINES

Sue Ellen Haupt [1,2] , Susan W. Stewart [2] , Julia A. Cole [2] ,
Frank J. Zajaczkowski, and Kerrie J. Schmehl [2]
[1] National Center for Atmospheric Research, Boulder, Colorado
[2] The Pennsylvania State University, University Park, Pennsylvania

1. INTRODUCTION

A recent development in wind energy is to site small wind turbines on or near buildings. This approach has the advantages of generating power at the point of use, integrating energy generation with other land uses, and harvesting accelerated wind power enhanced by building geometry. Some of the initial studies, however, did not attempt to optimize the location of the turbine on the building and the power production results were disappointing.

This purpose of this study is to simulate the potential wind power density around buildings using high fidelity computational fluid dynamics (CFD). Our approach is to model flow around buildings using very fine scale meshing techniques and apply a Detached Eddy Simulation model, which blends Reynolds Averaged Navier Stokes (RANS) modeling in the surface layer where the mesh is the finest as well as in the far field with Large Eddy Simulation (LES) in the separated regions detached from the building and in its wake. By employing this DES technique with a highly refined grid around a building and varying the wind direction, we are able to produce maps of power density in the vicinity of the building.

This modeling approach is first applied to a cubical geometry for which we can validate the CFD results with field measurements. We additionally model a slant roofed building to study the power density around typical residential buildings. Finally, we study the power density in a DES simulation of an urban environment to determine the impact of upstream buildings on the power density of those buildings in its wake.

*Corresponding author address: Sue Ellen Haupt, Research Applications Laboratory, National Center for Atmospheric Research, Boulder, CO 80301; e-mail: haupt@ucar.edu

2. BACKGROUND - BUILDING INTEGRATED WIND ENERGY

Compared to conventional fuel based energy resources, renewable energy generation technologies require considerable land area as the resources are extracted in real-time (and therefore sustainably) from the environment. However, there are many opportunities for integrating renewable energy technologies with land already being used for other purposes. For instance wind turbines have been successfully integrated on agricultural farms as have photovoltaics on building roofs. Similarly, wind turbine technologies have more recently been seen placed on top of buildings or integrated into the building design itself. However, a survey of the existing literature makes it clear that current installations of building integrated wind turbines are not taking into account specific features of the flow about the structures for either the turbine design or for siting for maximum performance. For instance, The Warwick wind trials in 2007-2008 in the UK analyzed the performance of 26 horizontal axis wind turbines mounted on buildings and found a capacity factor of only 4% (Warwick Wind 2009). While these turbines are generally operating as expected on their rated power curve, they are not experiencing as much wind as had been anticipated (BuildingGreen 2009). In addition, issues such as whether horizontal shaft turbines versus vertical shaft turbines are more applicable for integrating with buildings are open questions. To assess these issues scientifically and to use best engineering practices in designing the turbines requires careful analysis of the interaction of the building with the atmospheric flow. This process should begin with analyzing and correctly modeling the wind inlet profile. Such a profile depends on factors such as the wind speed, wind direction, atmospheric stability characteristics, surface roughness, and proximity to geophysical or man-made structures. It should then progress to full CFD analysis of specific features near building flows.

3. CFD METHODOLOGY

As a first validation exercise, we model flow around a 6 m cube. The experiments performed by Richards, et al. (2000, 2001, 2002, 2004, 2005) are modeled here with CFD using both the standard DES methodology with a Spalart-Allmaras turbulence model (Spalart et al. 1997) and a modification known as Zonal DES (ZDES) (Slimon 2003). The computational domain, shown in Fig. 1, features a 6 meter, surface-mounted cube situated within a domain that is 100 meters high. This domain height accommodates the experimentally measured atmospheric boundary layer (ABL) profile described in detail by Richards and Hoxey (2005).

3.1 Acusolve

We use the commercial flow code, AcuSolve™, as our computational engine. This solver is an incompressible, finite element code that offers several turbulence modeling options (Acusim 2005). AcuSolve™ allows various implementations and the ability to customize the modeling strategy. Our RANS closure is the Spalart-Allmaras (SA), one-equation turbulence model (Spalart et al. 1997) The SA model relates the eddy diffusivity, ν_T, to a computed diffusivity, $\tilde{\nu}$, that satisfies the transport equation. The SA model diagnoses the time scale of the turbulence from the mean field vorticity and chooses the characteristic length as the maximum distance to the wall. The model constants and functions are tuned to data.

3.2 Detached Eddy Simulation (DES)

For the current study, we use the DES model to compute the flow. DES is a hybrid statistical/eddy-resolving technique that harnesses the fidelity of large eddy simulation (LES) in regions of massive separation, like the separated flow downstream of the cube, while retaining much of the computational efficiency of RANS near boundaries and away from regions of interest. DES discriminates the LES and RANS regions by choosing a characteristic model length scale, $\tilde{d}$, that is the smaller of the characteristic grid scale, $C_{DES}\ \Delta$, and the local RANS length scale, d:

$$\tilde{d} \equiv \min(d, C_{DES}\Delta) \qquad (1)$$

where C_{DES} is an adjustable constant and $\Delta \equiv \max(\Delta x, \Delta y, \Delta z)$. When Δ << d, the DES subgrid model becomes a Smagorinsky-type LES. Likewise, when Δ >> d, the model remains RANS. Otherwise, the DES model blends the RANS and LES behaviors. Strelets (2001) describes how DES can be implemented for an arbitrary turbulence model and provides examples showing improved turbulence statistics over RANS predictions in regions of massive separation. AcuSolve™ implements the one equation Spalart-Allmaras turbulence model with curvature corrections in its RANS mode. Its DES implementation, therefore, follows the original prescription (Spalart et al. 1997).

3.3 Grids

The computational mesh is a high resolution, hybrid tetrahedral-prism unstructured grid. This mesh was generated with Ansys Icem CFD. Prism layers were extruded from solid walls to provide better modeling of near-wall physics than tetrahedrons. A near wall spacing of 0.003 m (about 300 wall units) was used in grid construction and a grid expansion rate of 1.2 was enforced in the wall normal direction yielding a total of 22 prism layers. Tetrahedral elements surround the prism layers. The size of the elements is limited to no larger than 0.85 m in the density region surrounding the cube. The farfield elements are allowed to grow to a maximum of 2.35 m. This high resolution grid contains 3.4 million elements. Figure 1 displays the grid. A top view (1a) indicates a refinement region surrounding the cube. A side view (1b) shows a cut plane through the center of the cube and a blow-up (1c) indicates the refinement of the prism layers. Wall functions are applied to enforce a smooth transition between the linear and logarithmic shear regions.

A grid study was accomplished to assure us that the computational mesh is sufficiently fine (Haupt et al. 2011).

3.4 Boundary Conditions and Implementation

Inflow conditions were extracted from the Silsoe full scale experimental data. Profiles of the inflow velocity and eddy viscosity are shown in Figure 3. The eddy viscosity was diagnosed from the measured turbulence intensities and length scales (Richards et al. 2005). Thus, both velocity and turbulence profiles are matched to the full scale data. In the experimental case, a reference

velocity at cube height was found to be ~10 m/s. The Reynolds number based on this reference and the cube height is $\mathrm{Re} = 4 \times 10^6$. An exit condition is used at the downstream boundary that allows vortical structures to advect out of the domain without unphysical pressure reflections. Symmetry conditions are imposed on the upper and side boundaries.

The Acusolve model with DES implemented was run in unsteady mode. Selecting a time step of 0.1 seconds gives a maximum Courant-Friedrichs-Lewy (CFL) number of 1 in the wake for the BASE grid. The BASE model was run for over 8000 time steps. The first 1400 steps are discarded from the analysis. To derive pressure coefficients, we select pressure profiles along the streamwise and cross-stream lines corresponding to the same distances measured in the Silsoe full scale field experiments. Such profiles are derived at 1000 step intervals and averaged for inclusion in the plots presented below.

The implementation described here proved to be successful at reproducing the observed experimental results (Haupt et al. 2011). These simulations were compared in terms of pressure coefficient profiles over several transects around the cube, modeled wind speed compared to several measurement points on and near the cube, and the separation and reattachment distances compared to those observed. These simulations performed at least as well as previously reported computational studies on most of these metrics, and in many cases better. This validation exercise provides us with confidence that similar setups and model simulations are similarly valid.

3.5 Varying Inflow Angle

For the cube shape, the model was run with three inflow angles of 0, 22.5 and 45 degrees. Using properties of symmetry, this allowed for an assessment of the flow over the entire structure throughout 360 degrees of incident wind flow (in 22.5 degree bins). We additionally modeled a building with a pitched roof (Figure 3). For the case of the pitched roof building, five inflow directions (0. 22.5, 45, 57.5, and 90) were needed to assess the full 360 degrees of wind conditions via symmetry.

3.6 CFD Results

Figure 4 and Figure 5 show the time averaged power density in the flow over the cubical building and the pitched roof building for 0 and 45 degree inflow angles, respectively. In the 0 degree case, the slant roof seems to cause less turbulent mixing over the front portion of the roof but it also induces an enhanced disturbance in the wake. Along the centerline of the building, the pitched roof shows an advantage for wind power density over the flat roof in the 0 to 1 m range as will be quantified in Table 1 in the next section. For the 45 degree case, the increase in power density seen just above the ridge line of the pitched roof is much more distinct than in the center of the flat roof structure. This also indicates a higher wind shear condition, which will have structural implications for a turbine in this environment.

Figure 6 demonstrates the impact that an upstream urban environment may have on the incoming flow to a building. It can be seen in this figure that buildings downstream from the leading edge of the incoming flow may severely limit the wind power density seen by buildings downstream. Several sources mention that these upstream /downstream effects should be considered within 20 times the height of the building being considered for a wind turbine installation to properly account for the losses the wakes that other buildings could cause. These effects have not been considered in the wind power mapping analysis, but should be a consideration in terms of selecting a proper site (building) for a wind turbine.

4. WIND POWER MAPPING

4.1 Methodology

Twenty-seven locations over top of each building type were assessed in the mapping study. These points consisted of nine points directly above the surface of the building, nine points 1 m above the surface and an additional nine points 2 m above the surface (see Figure 7). The specific layout and numbering of these points for the cube and the pitched roof shapes studied are shown in Figure 8.

The local wind velocity resulting from the CFD simulations at each one of these data points and for each wind inflow angle was recorded with the incident 10 m/s free stream wind velocity. Using symmetry, the wind speed that would result from the wind blowing from sixteen different compass directions (22.5 degree bins) was determined for each location. Using this information, the weighted-sum power density (power per unit area, $^1/_2\ \rho V^3$) was calculated for each point including an annual directional inflow variation determined by a wind rose.

The ensuing analysis is not directly comparable to a typical wind resource assessment as the upstream velocity for the CFD studies was a constant 10 m/s. For reference, the wind power density for a constant 10 m/s wind condition would be 612.5 W/m^2 (with an air density of 1.225 kg/m^3). If 10 m/s were instead an average velocity for a site that experienced a Rayleigh distribution (a Weibull distribution with a shape factor of 2), the annual average wind power density would be 1088.9 W/m^2. The inclusion of the wind distribution nearly doubles the available power in the wind because of the cubic relationship between wind speed and power. The times of the year in which the wind speed is higher than the average far outweigh the times of the year in which the wind is less than the average speed. Therefore the addition of a wind distribution to this analysis, at the same average wind speed, would increase the resulting average annual power densities. That said, a 10 m/s annual average wind speed is extremely high, so for reference, the average annual wind speed for the constant wind condition of 10 m/s is approximately equal to a site with a Rayleigh distribution and an annual average wind speed of 8 m/s, which is a bit more realistic, but still high for an urban area.

Generally, it was determined that local velocities over the building vary linearly with the incoming velocity (with Reynolds number), with the exception of right along the building surface (no slip condition) and above the center of the building. With this information an extension can be made to determine the local wind speeds for a site with a given wind distribution as well.

A variety of wind roses were analyzed to assess the impact of the directional variability of the wind on the performance of wind turbine devices at the locations above the building described earlier. Specifically, these wind roses represent several predominant scenarios: ridge top, land-sea, off-shore, and suburban. Here we report on the off-shore scenario.

4.2 RESULTS

Figure 9 shows the resulting wind power maps for the pitched roof and cube cases for each wind rose condition. There are several interesting results from these maps, but a primary value is in the methodology used, which can be applied in the assessment of wind resources for potential turbine installations on buildings.

For each of the wind rose conditions considered, the wind power at the surface of the roof is very nearly zero. This is due to the no slip condition on the roof. This case was, however, included here because there are several turbine manufacturers who have designed a turbine for use along the parapet of the building. While the wind power densities are much lower than those found at the 1 m and 2 m elevations, there is a peak in all of the scenarios at the 0 m level which may be of use in finding the “sweet” spot for this type of parapet mounting. In comparing the results from the cube shape versus the pitched roof, it can be seen that while there are higher maximum power density locations on the pitched roof there are also much lower minimum power density locations. Thus, although the power output may be greater for an installation on a building with a pitched roof if sited correctly, it is also possible for the turbine to perform significantly worse.

5. CONCLUSIONS AND PROSPECTS

The prospect of a thriving building integrated wind industry remains to be seen. While installations have occurred around the world, the siting process has proven to be quite difficult with few rules of thumb and a plethora of safety issues not well understood. There is very little work in the literature that analyzes the detailed flow conditions around buildings from a perspective of assessing wind power.

This study aimed to pull together elements of CFD with wind site assessment techniques to provide some quantification to the most suitable locations for extracting wind power from the area over two relatively basic building shapes in idealized upstream flow conditions. The goal is to move towards developing rules of thumb for proper siting of wind turbines on buildings. It was found that the wind direction variation has a significant impact over the optimal location of a wind turbine on a building in the region near the surface of the building as well as 1 m above the building. However, once a distance of 2 m of the building is reached (or 1/3 of the building height) the center of the building is the optimal location for all scenarios investigated. This indicates a very high wind shear condition in the lower layers of the flow over the center of the building. Also, the pitched roof scenarios achieved higher optimum power density values, typically along the ridge line of the roof, but there were also lower lows in other areas of the flow over the building than seen for the cubical shape

Acknowledgements: This research was supported by the Applied Research Laboratory.

The authors also thank ACUSIM Software, Inc. for supporting this work through licensing and technical assistance.

References

ACUSIM Software, 2008: *AcuSolve Command Reference Manual*, Version 1.8, 462 pp.

BuildingGreen.com, 2009: The Folly of Building-Integrated Wind, Environmental Building News. May 1, 2009.

Haupt, S.E., F.J. Zajaczkowski, and L.J. Peltier, 2011: Detached Eddy Simulation of Atmospheric Flow about a Surface Mounted Cube at High Reynolds Number, *J. Fluids Eng*., in press.

Long, K.J., F.J. Zajaczkowski, S.E. Haupt, and L.J. Peltier, 2009: Modeling a Hypothetical Chlorine Release on a College Campus, *Journal of Computers*, **40**, 881-890.

Lyons, D.C., L.J Peltier., F.J. Zajaczkowski, and E.G. Paterson, 2009: Assessment of DES models for separated flow from a hump in a turbulent boundary layer. *J Fluids Eng.*

Richards, P.J., and Hoxey, R.P., 2000: Spectral models for the neutral atmospheric surface layer, Journal of Wind Engineering and Industrial Aerodynamics, **87**, pp. 167-185.

Richards, P.J., Hoxey, R.P., and Short, L.J., 2001: Wind Pressures on a 6m Cube, Journal of Wind Engineering and Industrial Aerodynamics, **89**, pp. 1553-1564.

Richards, P.J., and Hoxey, R.P., 2002: Unsteady Flow on the Sides of a 6m Cube, Journal of Wind Engineering and Industrial Aerodynamics, **90,** pp. 1855-1866.

Richards, P.J., and Hoxey, R.P., 2004: Quasi-steady Theory and Point Pressures on a Cubic Building, Journal of Wind Engineering and Industrial Aerodynamics, **92**, pp. 1173-1190.

Richards, P.J., Hoxey, R.P., and Short L.J., 2005: A 6 m cube in an Atmospheric Boundary Layer Flow. Part 1. Full-Scale and Wind Tunnel Results. Wind and Structures, **5**, pp. 165-176.

Slimon, S., 2003: Computation of internal separated flows using a Zonal Detached Eddy Simulation approach, Proceedings of IMECE'03, IMECE2003-43881.

Spalart, P.R., Jou, W.-H., Strelets, M., and Allmaras, S.R., 1997: Comments on the Feasibility of LES for Wings, and on a Hybrid RANS/LES Approach, 1st AFOSR Int. Conf on DNS/LES, Rustin, LA. In *Advances in DNS/LES*, C.Liu & Z.Liu Eds., Greyden Press, Columbus, OH, pp. 137-147.

Strelets, M., 2001: Detached Eddy Simulation of Massively Separated Flows, AIAA 2001-0879.

Warwick Wind, 2009: http://www.warwickwindtrials.org.uk/resources/Warwick+Wind+Trials+Final+Report+.pdf

Figures

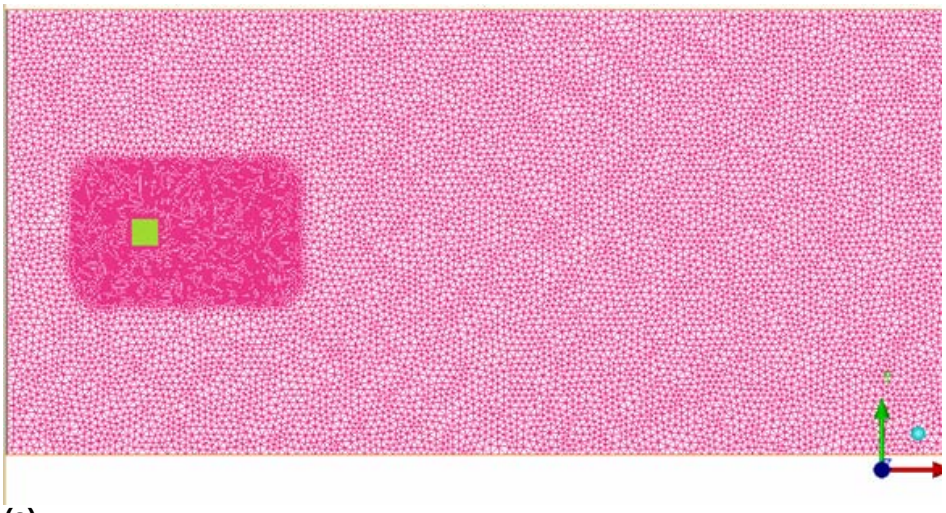

(a)

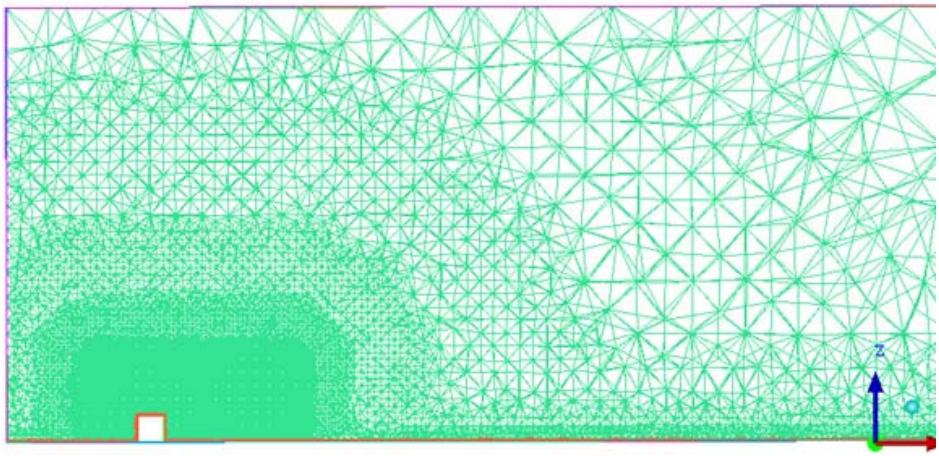

(b)

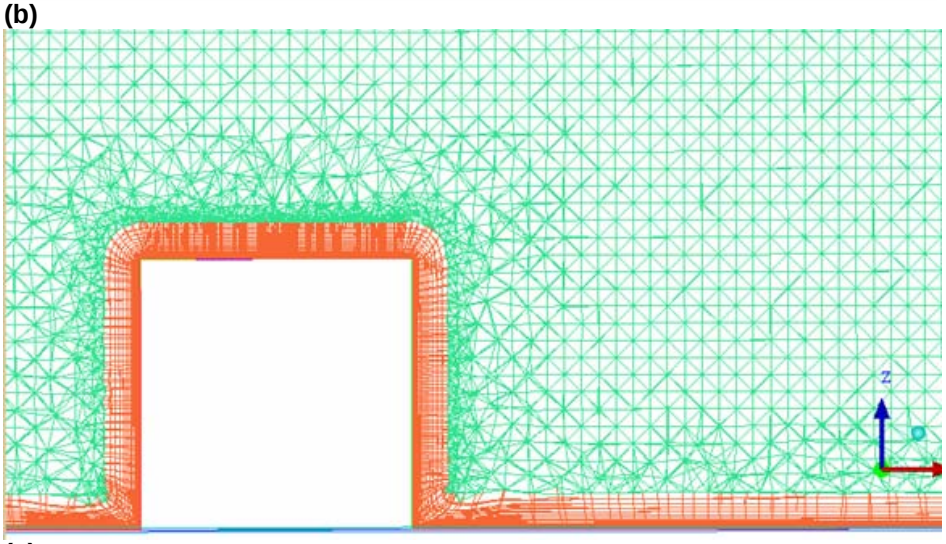

(c)

Figure 1. Computational mesh for the BASE case runs. a) top view showing the refinement region, b) side view through the cube, c) close-up of the side view indicating the prism layers near the wall.

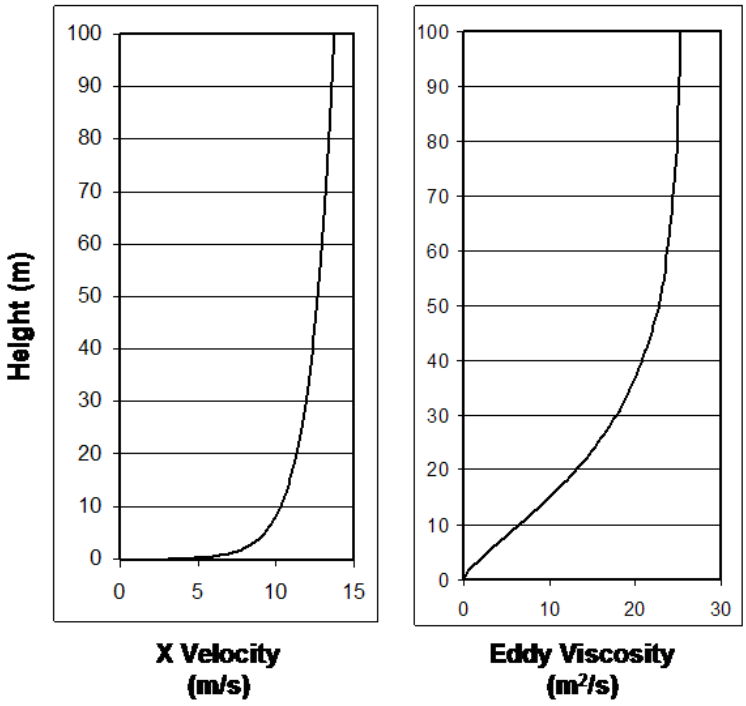

Figure 2. Inflow conditions fit from experimental data.

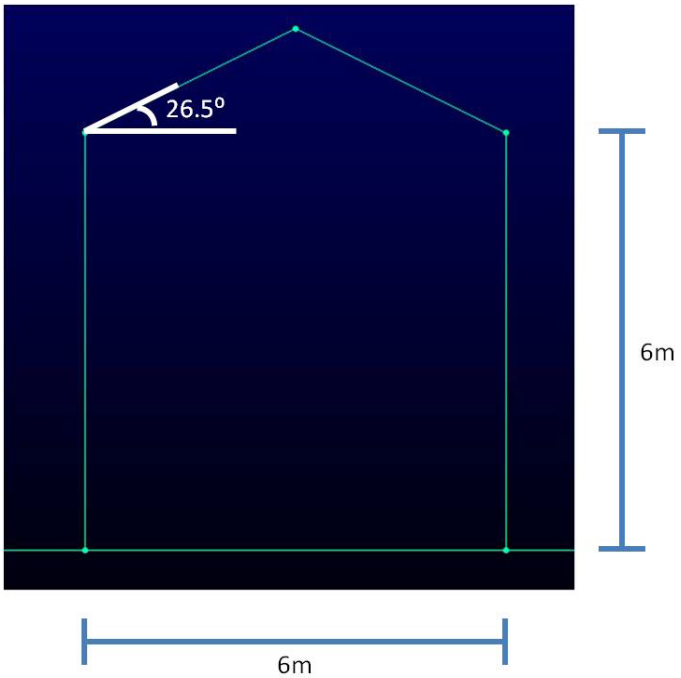

Figure 3. Pitched Roof Configuration

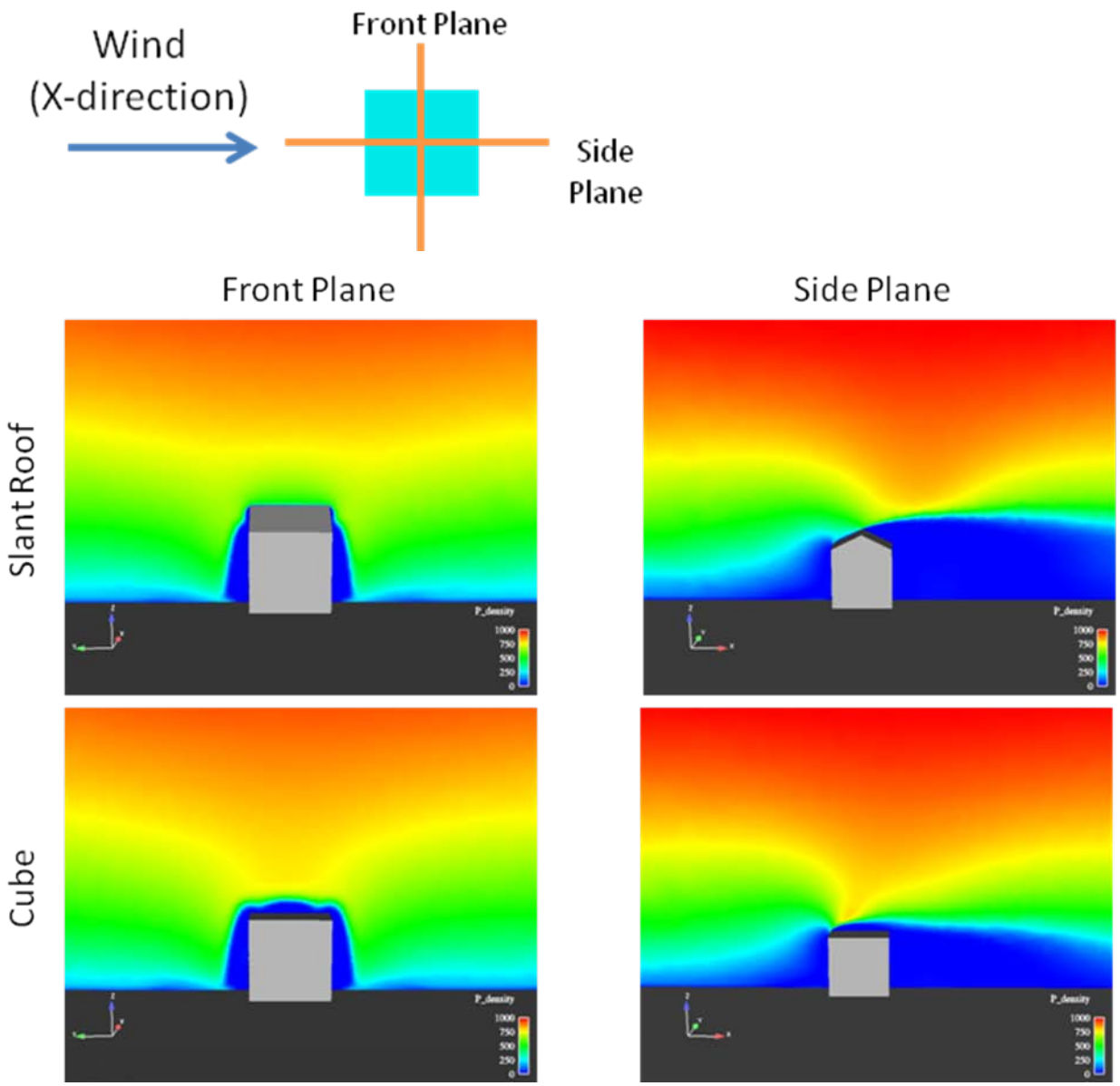

Figure 2. Slant roof vs. cube CFD results for 0 degree Inflow. Front plane and side plane views.

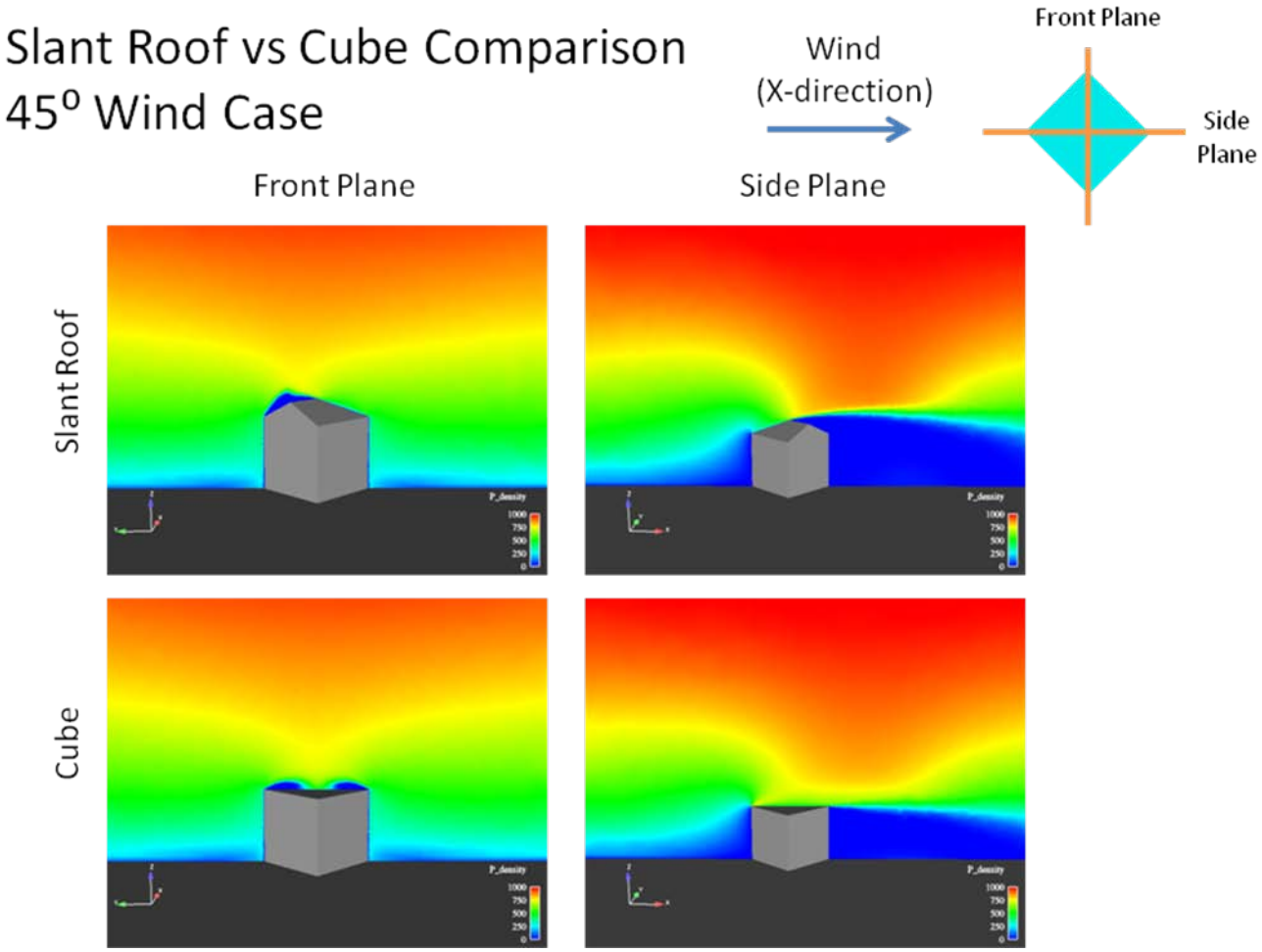

Figure 3. Slant roof vs. cube CFD results for 45 degree Inflow. Front plane and side plane views.

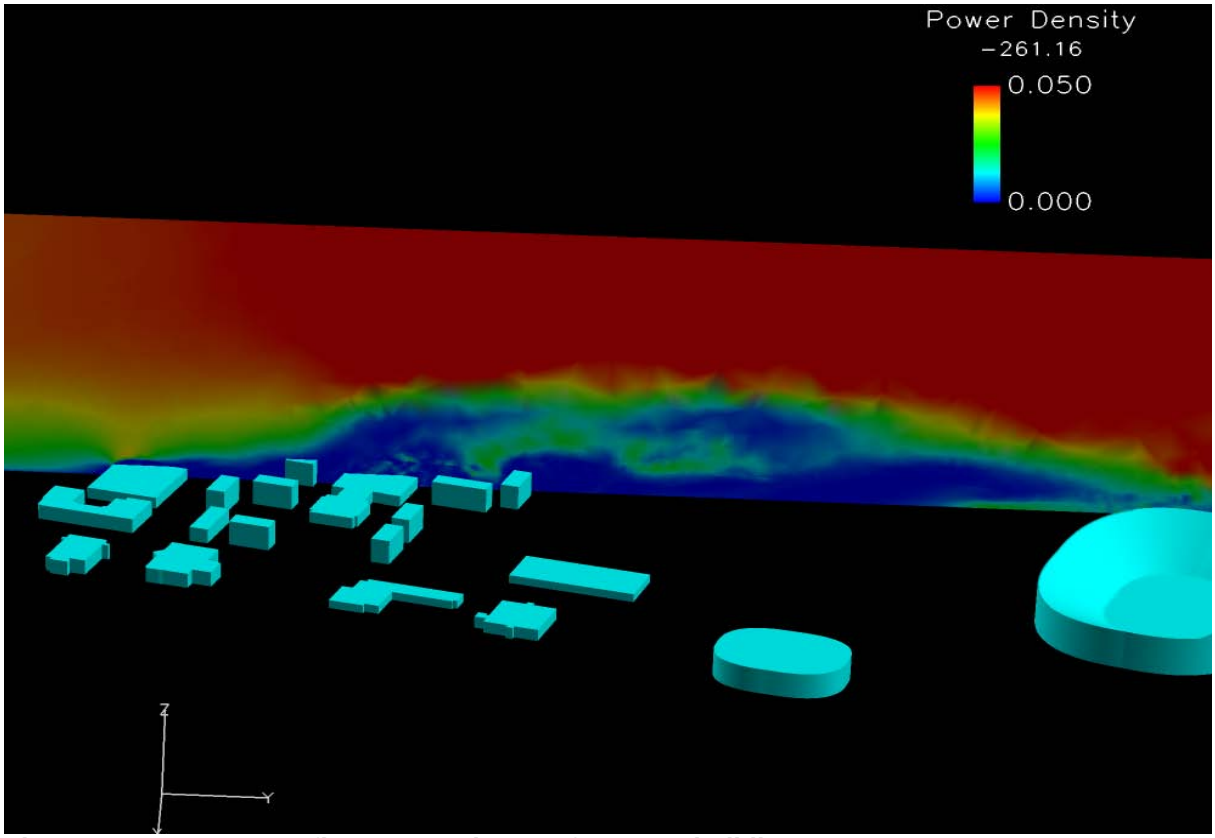

Figure 4. Instantaneous flow over a cluster of campus buildings.

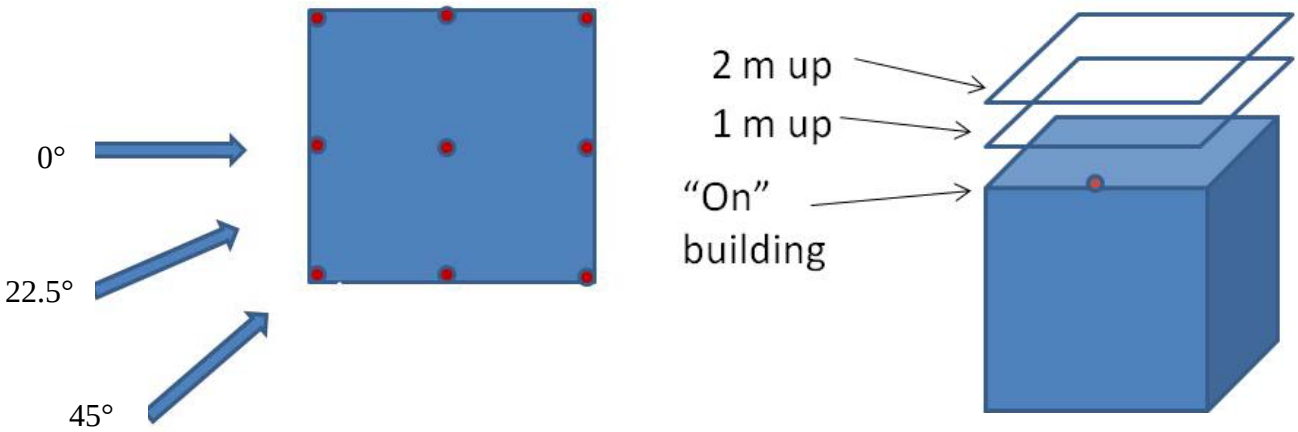

Figure 5. Layout of wind power mapping points and incoming wind directions modeled.

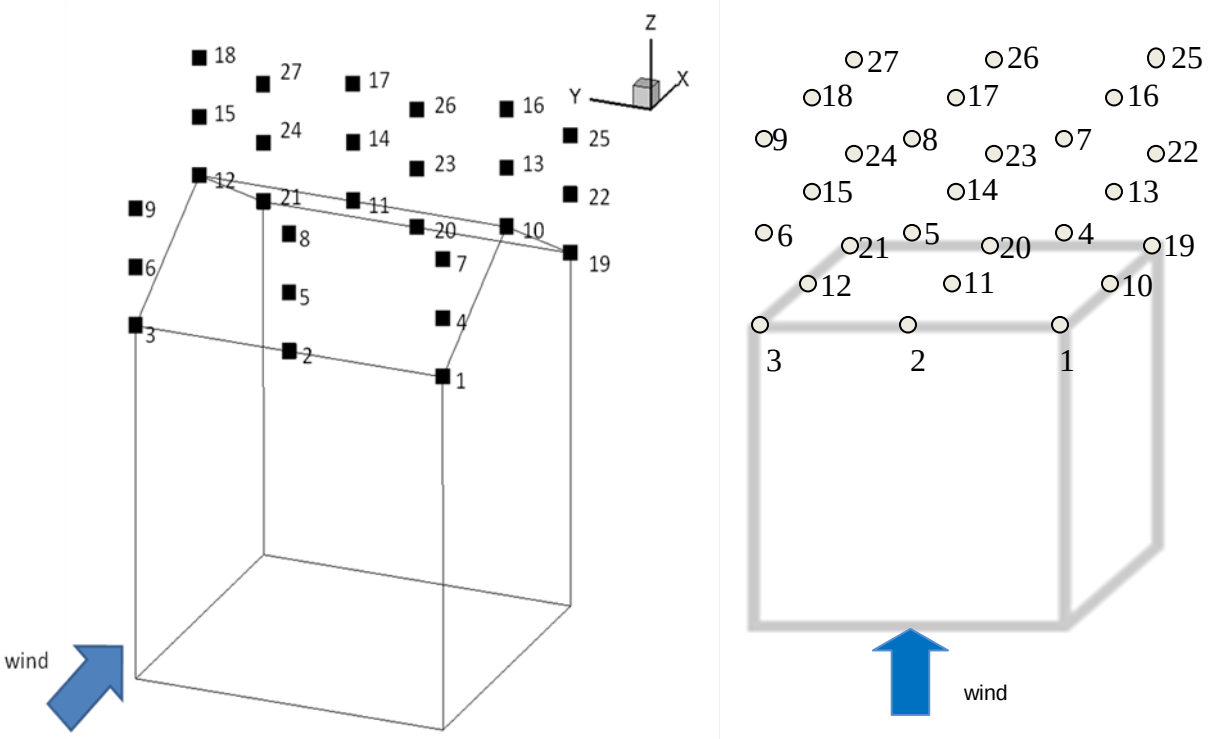

Figure 6. **Location of wind power mapping points on pitched and square roof structure.**

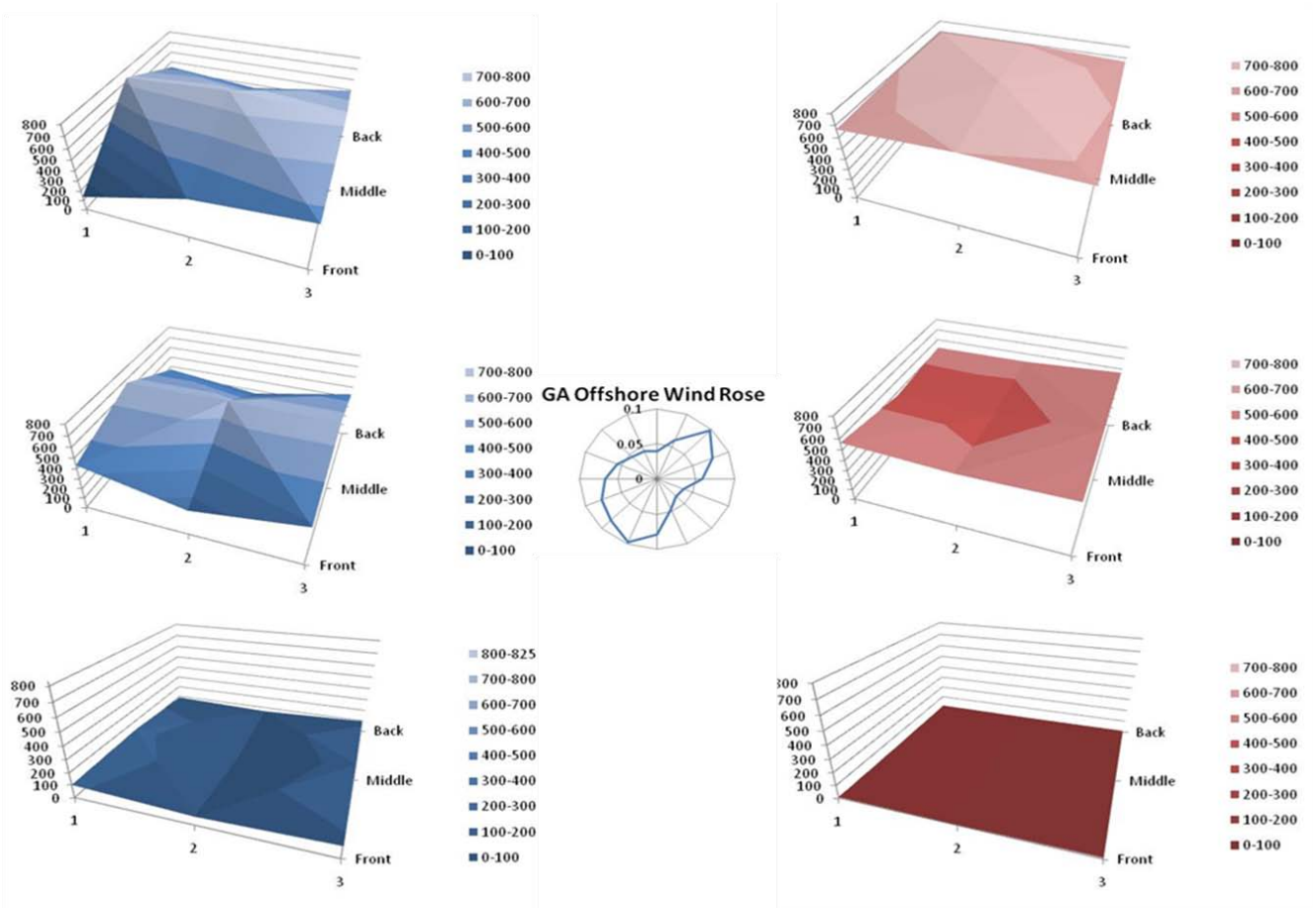

Figure 9. Wind power maps for a pitched roof and a cube structure in a wind distribution such as that found along the coast of Georgia.